Limit Cycle Analysis of Large Space Telescope with CMG Nonlinearity

B.C. Kuo* and G. Singh†
University of Illinois at Urbana-Champaign, Urbana, Ill.
and
S.M. Seltzer‡
George C. Marshall Space Flight Center, Ala.

The purpose of the investigation reported upon is to study the existence and characteristics of self-sustained oscillations in the dynamic behavior of the Large Space Telescope (LST) system due to the presence of nonlinear gimbal friction in the control moment gyroscopes (CMG's). A continuous data single-axis model of the LST is considered. A solid friction model is used to represent CMG gimbal friction. A rigorous mathematical model is derived for use in a continuous describing function analysis. Conditions for self-sustained oscillations are then determined.

Introduction

THE purpose of this investigation is to study the existence of self-sustained oscillations in the Large Space Telescope (LST) system due to the presence of nonlinear gimbal friction of the control moment gyroscope (CMG).[1,2] A continuous-data, single-axis model of the LST control system is considered with the CMG nonlinearity modeled as shown in Fig. 1. One of the major differences in the modeling of the dynamics of the CMG is in the accurate representation of the nonlinear friction characteristics of the CMG. The running friction of the gimbal axis consists of both tachometer brush friction and the hysteresis drag which is associated with the brushless dc permanent-magnet torque motor. These frictional torques do not have significant effect on large motion gimbal-rate control loop performance other than the power loss required to overcome the drag torque. However, the accurate representation of these torques for small motion has a pronounced influence on the gimbal-rate control loop small-motion performance. Whereas these effects have been second order for most previously reported-on systems, their effect is significant for the highly accurate performance requirements of LST. Therefore, the accurate modeling of these torques is essential in predicting the existence of limit cycles and the control loop response to very low-level commands.

Using the solid friction model reported in Ref. 3, a mathematical model of the CMG friction nonlinearity is derived for continuous describing function analysis. It is shown that the input-output characteristics of the nonlinearity are only a function of the amplitude A of the input sinusoid and the nonlinearity parameters. A continuous describing function $N(A)$ is derived for the CMG nonlinearity using the analytical frictional torque expression, and conditions for self-sustained oscillations are determined analytically. Digital computer simulations have been carried out to corroborate the analytical results.

Single-Axis Model of the LST Control System

A simplified single-axis model of the LST fine-pointing control system is shown in Fig. 1. The block diagram represents a simplified version of the LST control system obtained by neglecting the bending modes of the vehicle and the current loop and back emf of the CMG. However, the results of this paper can be extended to more complex system models without difficulties.

The transfer function $G_5(s)$ denotes the vehicle dynamics of the LST as a single inertia I. The dynamics of the CMG are also modeled by a single inertia with the transfer function $G_4(s)$. The transfer functions $G_2(s)$ and $G_3(s)$ represent the CMG gimbal controller. The torsional feedback of the CMG output axis has been neglected. The block N denotes the CMG gimbal friction nonlinearity. The assumed characteristics of the nonlinearity are described and mathematically treated in the next section.

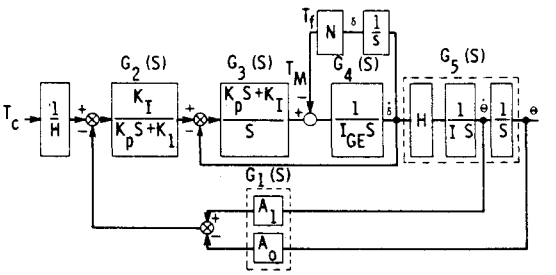

Fig. 1 Single-axis model.

Table 1 LST system parameters

Variable	Description	Magnitude
H	CMG angular momentum	271 Nms
I	vehicle inertia	1.354×10^5 Nms^2
I_{GE}	gimbal inertia	5.0 Nms^2
K_I	gimbal rate loop integral gain	1.354×10^4 Nm
K_p	gimbal rate loop gain	379 Nms
A_0	vehicle controller coefficient	2×10^4(rad·s)$^{-1}$
A_1	vehicle controller coefficient	3×10^3 (rad)$^{-1}$
ϵ	error input command to CMG	0.136 Nm
T_f	torque output of nonlinearity	Nm
T_{f0}	running friction torque	0.136 Nm
γ	gimbal bearing parameter	1.871×10^5(Nms)$^{-1}$
δ	gimbal position	rad
$\dot{\delta}$	gimbal velocity	rad/sec
θ	vehicle position	rad
$\dot{\theta}$	vehicle velocity	rad/sec

Presented as Paper 74-874 at the AIAA Mechanics and Control of Flight Conference, Anahaim, California, August 5-9, 1974; submitted September 3, 1974; revision received March 13, 1975.

Index categories: Spacecraft Attitude Dynamics and Control; Navigation, Control, and Guidance Theory.

*Professor, Department of Electrical Engineering. Member AIAA.

†Research Assistant Professor, Department of Electrical Engineering. Member AIAA.

‡Chief, Pointing Control Systems Branch. Associate Fellow AIAA.

The controller for the LST vehicle is represented by the transfer function $G_1(s)$ which is of the proportional-plus-derivative (attitude-attitude rate) type. Since the objective of this paper is not the design of the LST system, this conventional form of $G_1(s)$ is chosen for the purpose of computer simulation. It can be shown that the controller $G_1(s)$ is optimal in the sense of pole-placement design without the nonlinearity. Simulation results show that the system's response is quite satisfactory with this controller.

A list of symbols that describe the LST system variables and parameters, together with their numerical values, is given in Table 1.

Mathematical Model of the CMG Frictional Nonlinearity

The running friction of the gimbal axis of the CMG consists of both the tachometer brush friction and the hysteresis drag which is associated with the brushless dc permanent-magnet torque motor. These frictional torques do not have significant effect on large-motion gimbal-rate control loop performance other than through the power loss required to overcome the drag torque. In ordinary control system practice, these frictional characteristics can be either modeled as viscous or coulomb frictions or totally neglected if the amplitude of the frictional torque is relatively small. However, because of the fine-pointing accuracy and stability requirements of the LST system, accurate representation of the frictional torque becomes extremely important. For fine-pointing studies of the LST, the accurate modeling of the frictional torques is essential in predicting the existence of limit cycles and the control loop stability when the system is subject to a very low-level disturbances and commands.

In this section, a mathematical model of the CMG friction nonlinearity is derived, based on the Dahl solid friction model.[3,4] The purpose of this model is that it can be used for the continuous-data describing function analysis of the nonlinear LST system.

A mathematical and simulation model of solid friction, such as that encountered in a bearing, was reported in Ref. 4. Subsequent experimental studies have indicated that the frictional characteristics of the CMG can be approximated by this solid friction model. A more accurate model that has the same general characteristics as the one used herein has recently been developed.[5] However, since it is not precisely the same as that used in Refs. 3 and 4, studies are now underway at NASA's Marshall Space Flight Center, and by the co-authors of Ref. 5 and other CMG developers, to develop an understanding of the effects of the more precise model on CMG and LST dynamics. If CMG output shaft friction torque vs shaft attitude (δ) or attitude rate ($\dot{\delta}$) were plotted, it could be seen that the simplified model used herein yields the envelope of the plots obtained with the model of Ref. 5. Hence, it is felt (but as yet unproven) that the limit cycle predictions yielded by using the simplified model are approximately correct.

As indicated in Refs. 3 and 4, the key to the simulation model is that the frictional torque T_f is a function of the CMG shaft displacement δ and can be differentiated with respect to time. Thus,

$$(dT_f/dt) = (dT_f/d\delta)\,(d\delta/dt) = T_f'\dot{\delta} \tag{1}$$

The frictional torque T_f can be generated by integrating both sides of Eq. (1) with respect to t.

In the simulation model, T_f' is generated by a function generator with input T_f. The output of the function generator is multiplied by $\dot{\delta}$ to give the right-hand side of Eq. (1) which is then integrated to yield T_f. Figure 2 is a simulation diagram of the CMG friction nonlinearity. The input of the model is $\dot{\delta}$, and the output is T_f. The relays are necessary because T_f is sensitive to the sign of $\dot{\delta}$.

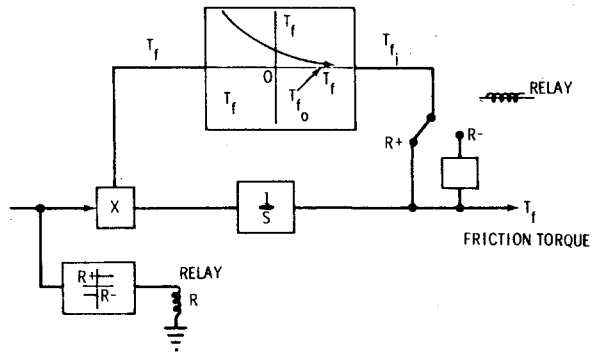

Fig. 2 Simulation of CMG friction nonlinearity.

It has been demonstrated experimentally that for solid rolling friction, the relation between T_f' and T_f may be approximated by a square-law expression

$$T_f' \approx \gamma(T_f - T_{f_0})^2, \quad T_f \le T_{f_0}$$
$$T_f' = 0, \quad T_f > T_{f_0} \tag{2}$$

where γ is a positive constant, and T_{f_0} is the normalizing factor of T_f. However, the frictional torque is also velocity ($\dot{\delta}$) dependent, as shown in Fig. 2. Therefore, Eq. (2) should be written

$$T_f' = \gamma(T_{f_i} - T_{f_0})^2 \tag{3}$$

where

$$T_{f_i} = T_f \operatorname{sgn}\dot{\delta} \tag{4}$$

Integrating both sides of Eq. (2), one obtains

$$\delta + C = -\gamma(T_f^+ - T_{f_0})^{-1}, \quad \dot{\delta} \ge 0 \tag{5}$$

and

$$\delta - C = -\gamma(T_f^- - T_{f_0})^{-1}, \quad \dot{\delta} \le 0 \tag{6}$$

where C is the constant of integration, and

$$T_f = T_f^+, \quad \dot{\delta} \ge 0$$
$$= T_f^-, \quad \dot{\delta} \le 0 \tag{7}$$

If one assumes a sinusoidal input for δ, such as

$$\delta = A\cos\omega t \tag{8}$$

then

$$C = A + [\gamma(R+1)T_{f_0}]^{-1} \tag{9}$$

$$R \equiv -a^{-1} + ((a^2+1)/a^2)^{1/2} \tag{10}$$

$$a \equiv 2\gamma A T_{f_0} \tag{11}$$

and solving Eqs. (5) and (6) for T_f, one obtains

$$T_f = T_f^+ = -[\gamma(A\cos\omega t + C)]^{-1} + T_{f_0}, \quad \dot{\delta} \ge 0$$
$$= T_f^- = -[\gamma(A\cos\omega t - C)]^{-1} - T_{f_0}, \quad \dot{\delta} \le 0 \tag{12}$$

Describing Function for the CMG Gimbal Friction Nonlinearity

In order to derive a describing function for the assumed CMG nonlinearity, one assumes a sinusiodal input to the

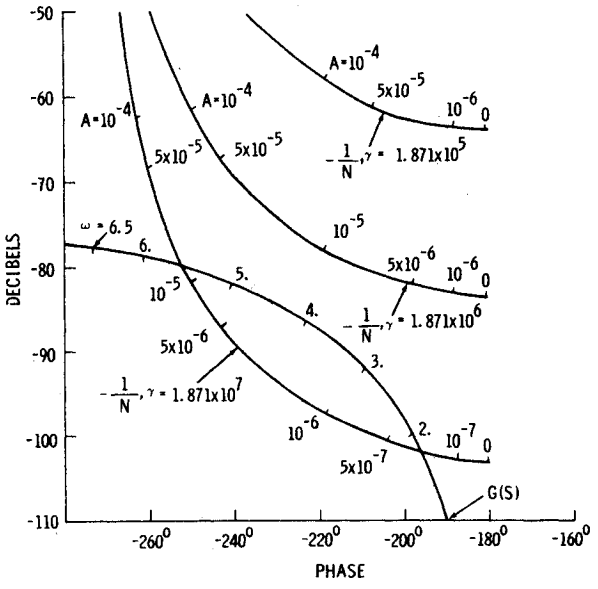

Fig. 3 $-1/N$ and $G(s)$ plots.

nonlinearity of the form of Eq. (8). The output of the nonlinearity, T_f, is approximated by the fundamental component of its Fourier series. Since the input-output relation of the nonlinearity is symmetrical about the zero-torque axis, there is no dc component in the series. Thus

$$T_f \approx T_1(t) = \bar{A}_1 \sin\omega t + \bar{B}_1 \cos\omega t \tag{13}$$

where

$$\bar{A}_1 = 1/\pi \int_0^{2\pi} T_f \sin\omega t \, d\omega t = 1/\pi \int_0^{\pi} T_f^- \sin\omega t \, d\omega t + 1/\pi \int_{\pi}^{2\pi} T_f^+ \sin\omega t \, d\omega t \tag{14}$$

$$\bar{B}_1 = 1/\pi \int_0^{2\pi} T_f \cos\omega t \, d\omega t = 1/\pi \int_0^{\pi} T_f^- \cos\omega t \, d\omega t + 1/\pi \int_{\pi}^{2\pi} T_f^+ \cos\omega t \, d\omega t \tag{15}$$

Equation (13) can also be written as

$$T_1(t) = (\bar{A}_1^2 + \bar{B}_1^2)^{1/2} \cos(\omega t - \phi) \tag{16}$$

where

$$\phi = \tan^{-1}(\bar{A}_1/\bar{B}_1) \tag{17}$$

or in phasor notation,

$$T_1(i\omega) = (\bar{A}_1^2 + \bar{B}_1^2)^{1/2} \exp[i \tan^{-1}(\bar{A}_1/\bar{B}_1)] = \bar{B}_1 - i\bar{A}_1 \tag{18}$$

The describing function is given by

$$N(A) = T_1(i\omega)/\delta(i\omega) = (\bar{B}_1/A) - i(\bar{A}_1/A) = N_1 + iN_2 \tag{19}$$

The coefficients $\bar{A}_1$ and $\bar{B}_1$ can be obtained by substituting Eq. (12) into Eqs. (14) and (15), respectively, and performing the appropriate integrations. The results are

$$\bar{A}_1 = -(4T_{f_0}/\pi) + 2\ell n[(C+A)/(C-A)]/\pi A\gamma = (2T_{f_0}/\pi a)\{\ell n[a + (a^2+1)^{1/2}]^2 - 2a\} \tag{20}$$

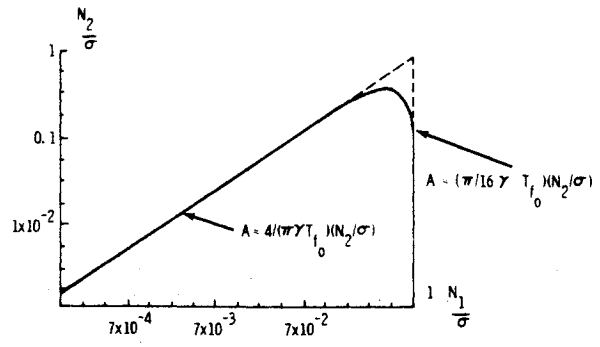

Fig. 4 Normalized Dahl describing function locus. Describing function asymptotes, note: Values for A are found from core curves 1 and 2, respectively, by reading the value of N_2/σ for the point in question and then applying the approximation indicated.

$$\bar{B}_1 = 2\{[C/(C^2-A^2)^{1/2}] - 1\}/\gamma A = (4T_{f_0}/a)\left[[a^2+a+1+(a+1)(a^2+1)^{1/2}]/2[a+(a^2+1)^{1/2}] - 1\right]^{1/2} \tag{21}$$

For stability analysis, it is of interest to determine the behavior of $-1/N(A)$. This may be computed readily by use of Eqs. (19-21). Figure 3 shows the magnitude (db) vs phase (deg) plots of $-1/N(A)$ for $\gamma = 1.871 \times 10^5$, 1.871×10^6, and $1.87 \times 10^7 (\text{Nms})^{-1}$, as the magnitude of A varies.

Figure 3 shows that as A approaches zero, the magnitude of $-1/N(A)$ in db approaches $20 \log_{10}[1/\gamma T_{f_0}]$ and the phase is $-180°$. This asymptotic behavior of $-1/N(A)$ for small values of A may be derived analytically by expanding the logarithmic term in Eq. (20) and using relations (7-9):

$$\lim_{A \to 0} (\bar{A}_1/A) = 0 \tag{22}$$

Similarly, by expanding the square-root term of Eq. (21) into a power series one obtains

$$\lim_{A \to 0} (\bar{B}_1/A) = \sigma \tag{23}$$

where

$$\sigma \equiv \gamma T_{f_0}^2 \tag{24}$$

Thus

$$\lim_{A \to 0} [-1/N(A)] = \lim_{A \to 0} \{-[(\bar{B}_1/A) - i(\bar{A}_1/A)]\}^{-1} = -1/\sigma \tag{25}$$

For large values of A, the value of C becomes

$$\lim_{A \to \infty} C = \lim_{A \to \infty} (A + 2/\gamma T_{f_0}) = \lim_{A \to \infty} [A] \to \infty \tag{26}$$

Then

$$\lim_{A \to \infty} (\bar{A}_1/A) = \lim_{A \to \infty} (-4T_{f_0}/\pi A) = -0 \tag{27}$$

and

$$\lim_{A \to \infty} (\bar{B}_1/A) = +0 \tag{28}$$

Thus

$$\lim_{A \to \infty} [-1/N(A)] = -i/0 \to \infty \underline{/-270°} \tag{29}$$

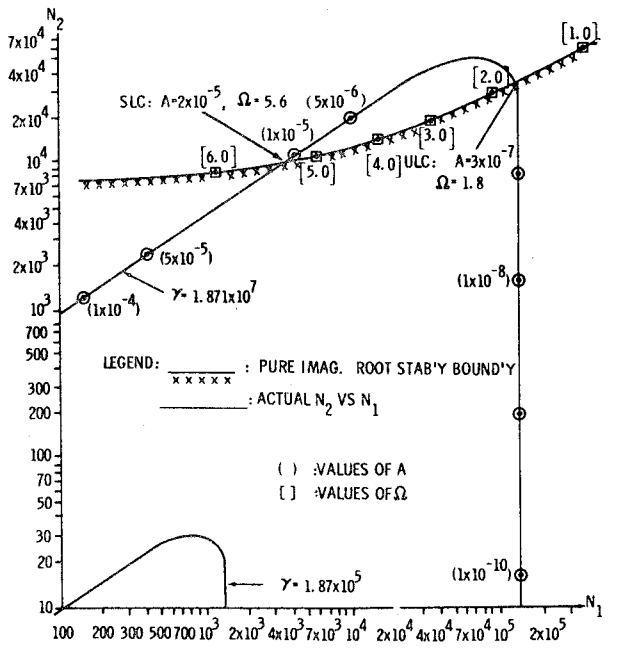

Fig. 5 N_1-N_2 parameter plane.

As shown in Fig. 3, the gain-phase plots of $-1/N(A)$ approach $\infty/\underline{-270^\circ}$ as $A\to\infty$ for all values of γ and T_{f_0}.

Alternately, a general map of N_2 vs N_1 (as a function of the argument A) may be developed for use in this and future limit cycle investigations for this particular form of nonlinearity (Fig. 4).[6] It is universal in the sense that it permits one to choose any design values for T_{f_0} and γ, and see their effect on the N_2 vs N_1 map.

Stability Analysis by Use of the Describing Functions

The system described in Fig. 1 appears to be suitable for describing function analysis because it is low-pass and the system parameters are assumed time-invariant. The condition for a self-sustained oscillation in a linear system with a nonlinearity is given by

$$1+N(A)G(i\omega)=0 \tag{30}$$

where $N(A)$ is the describing function of the nonlinearity and $G(i\omega)$ is the transfer function of the system which is seen by the nonlinearity. The solution of Eq. (30) can be obtained graphically by plotting the $G(i\omega)$ curve for the system and the $-1/N(A)$ curve for the nonlinearity. The point of intersection of these curves will yield the solution to Eq. (30). The magnitude and frequency of the oscillation corresponds to the values of A and ω at the solution point.

For the LST system in Fig. 1, the transfer function which the nonlinear element sees is

$$G(s)=\frac{Is^2}{II_{GE}s^4+IK_ps^3+IK_Is^2+K_IHA_Is+K_IHA_0} \tag{31}$$

The relevant portions of the frequency-domain plot of $G(s)$ are superimposed on the $-1/N$ curves of Fig. 3 in db vs phase coordinates. With $\gamma=1.87\times^{7}$, the $-1/N$ curve intersects the $G(s)$ curve at two points. The stable point for sustained oscillations is the one on the left at the higher frequency. The approximate magnitudes for frequencies of the oscillations are 3×10^{-7} rad and 1.8 rad/sec, respectively, for the unstable limit cycle, and 2×10^{-5} rad and 5.6 rad/sec, respectively, for the stable limit cycle. The curves in Fig. 3 also show that for γ considerably smaller than 1.871×10^7, the system will exhibit a stable response.

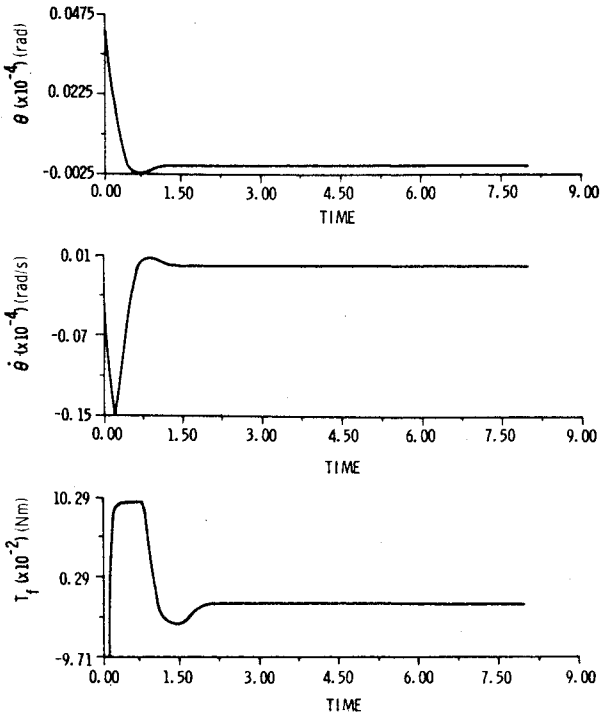

Fig. 6 Simulation ($\gamma=1.871\times10^7$).

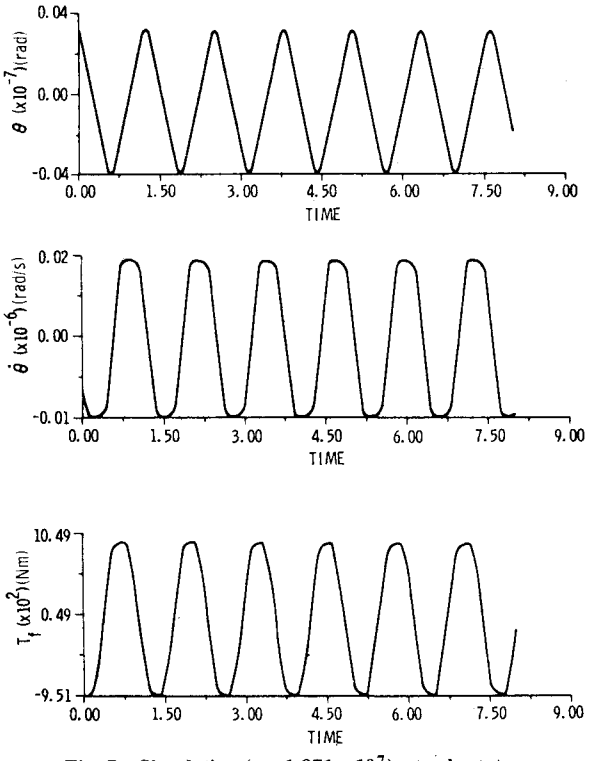

Fig. 7 Simulation ($\gamma=1.871\times10^7$): steady state.

Following the alternate approach begun in the previous section, limit cycle conditions and characteristics may be predicted using the parameter plane technique.[6] Specifically, one may place the describing function locus (Fig. 4) on an N_1, N_2 parameter plane stability map to analyze and predict limit cycle behavior. The result is portrayed on Fig. 5 and agrees with the stability analysis technique portrayed on Fig. 3.

Simulation

To corroborate these results, the LST system was simulated on a digital computer. The CMG friction nonlinearity was simulated as shown in Fig. 2. For the computer simulation,

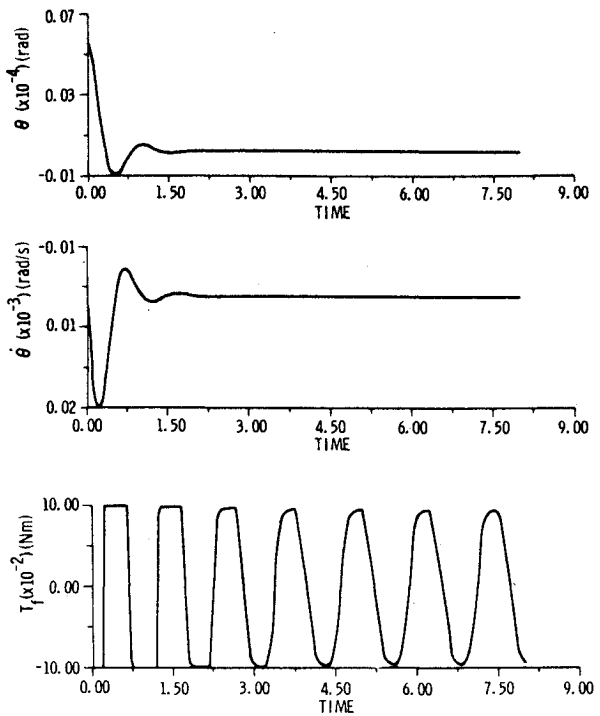

Fig. 8 Simulation ($\gamma = 1.871 \times 10^5$).

the input to the LST system, T_c, was set to zero, along with all of the initial states, except for the vehicle position, θ, which was set at 5×10^{-5} rad. This value was chosen so that the input signal to the nonlinearity, δ, would be large enough to cause the torque to saturate but not so large as to exceed the limiting value of the input signal.

The quantities plotted from the simulation runs are vehicle attitude and attitude rate, θ and $\dot{\theta}$, and friction torque, T_f. Figure 6 shows the plots with $\gamma = 1.871 \times 10^7$. It is observed from the plot of T_f in Fig. 6 that the system has a sustained oscillation. This oscillation is not seen on the other plots because of the large initial transients. For this reason, the vertical scale of the plot is adjusted (Fig. 7) to show the oscillations. The frequencies and magnitudes of oscillations obtained are quite close to the predicted values. The small discrepancy is partly attributed to the quantization caused by the nonlinearity implementation on the digital computer. Figure 8 shows the response plots with $\gamma = 1.871 \times 10^5$. As predicted, the system is stable for the lower values of γ.

Conclusions

For numerical values considered to be representative of the LST and its CMG's, analysis of the simplified continuous-data model with a solid friction CMG nonlinear characteristic indicates (and analogue simulation confirms) the absence of limit cycle behavior due to the CMG nonlinearity. It must be borne in mind that the analysis has not yet included the dynamic effects induced by the sampling phenomena of the onboard digital computer. Experience with past spacecraft would lead one to expect quantization, for example, to induce limit cycling of the plant.

References

[1] O'Dell, C.R., "Optical Space Astronomy and Goals of the Large Space Telescope," *Astronautics & Aeronautics,* Vol. II, April 1973, pp. 22-27.

[2] Proise, M., "Fine Pointing Performance Characteristics of the Orbiting Astronomical Observatory (OAO-3," AIAA Paper 73-869, Key Biscayne, Fla., Aug. 1973.

[3] Dahl, P.R., "A Solid Friction Model," TOR-158 (3107-18), The Aerospace Corporation, El Segundo, Calif., May 1968.

[4] Nurre, G.S., "An Analysis of the Dahl Friction Model and Its Effect on a CMG Gimbal Rate Controller," NASA TMX 64934, Oct. 1973.

[5] Rittenhouse, D.L. and Osborne, N.A., "Modeling of Friction and Its Effects on Fine Pointing Control," AIAA Paper 74-875, Anaheim, Calif., Aug. 1974.

[6] Seltzer, S.M., "Large Space Telescope Dynamics Induced by CMG Friction," *Journal of Spacecraft and Rockets,* Vol. 12, Feb. 1975, pp. 96-105.